

Loschmidt echo, emerging dual unitarity and scaling of generalized temporal entropies after quenches to the critical point

Stefano Carignano

*Barcelona Supercomputing Center, 08034 Barcelona, Spain**

Luca Tagliacozzo

Institute of Fundamental Physics IFF-CSIC, Calle Serrano 113b, Madrid 28006, Spain[†]

We discuss how all relevant objects involved in the calculation of the Loschmidt echo of a product state after a quench to a conformal invariant critical point can be predicted by using conformal field theories. We check such prediction with tensor networks finding excellent agreement. In particular we are able to predict and confirm that in such an out-of-equilibrium scenario, we observe an emerging dual-unitarity of the evolution. We also show how to extract the universal information of the underlying CFT from such out-of-equilibrium protocol, including, the central charge, the operator content, and the generalized temporal entropies. In particular we show that using state-of-the-art tensor networks algorithms such calculations only require resources that increase polynomially with the duration of the quench, thus providing an example of numerically efficiently solvable out-of-equilibrium scenario.

Introduction.— Strongly-correlated quantum systems still defy our understanding under many aspects. The situation is especially complicated out-of-equilibrium, where even the existence of non-ergodic phases such as the many-body localized phase is still highly debated [1, 2]. As a result, most of our understanding of the out-of-equilibrium dynamics emerges from either integrable models [3–6], conformal field theories [7–12], Floquet systems such as random circuits [13] or dual unitary models [14–18].

Dual-unitary models are particularly interesting since they provide an analytic framework for computing interesting quantities without being integrable and thus provide access to both ergodic and non-ergodic dynamics. Their main characteristic is that the dual unitarity constrains the dynamics to the light front and all correlations inside it vanish, thus providing the example of a dynamics with a single velocity. However until now they have been limited to Floquet dynamics, thus only providing infinite temperature steady states. Recently, simple dual unitaries have been used to construct toy models for holography which display emerging discrete Lorentz and conformal invariance [19].

Here we provide an example of the opposite relation, by showing that quenches described by conformal field theories provide examples of emerging dual-unitary dynamics in an Hamiltonian setting. The underlying mechanics is intuitive and clearly rooted to the presence of Lorentz invariance forcing a linear dispersion relation, with a single propagating velocity of excitations. However, to the best of our knowledge such connection was not made explicit before.

We obtain our results by characterising the return probability of an initial product state after a quench to

the critical conformal invariant point. We combine simple CFT calculations with tensor networks simulations to unveil all universal properties of such protocol. In particular, we show how to define a transverse transfer matrix (TM) whose spectrum becomes that of a unitary matrix that is dictated by the operator content of the CFT [20, 21]. We also show that the return probability contains the usual Casimir-like terms proportional to the central charge [22, 23]. Finally, we show that the generalized temporal entropy for the leading eigenvector of such TM is well described by the predictions obtained from holography that can be easily re-obtained from conformal field theories, as also shown in [24–30]. In order to check such predictions we provide tensor networks simulations based on our recently introduced algorithm¹ [36] of two exemplary minimal models, the Ising and the three-states Potts model, finding perfect agreement with the CFT predictions once the leading corrections to scaling are taken into account.

With our calculations we also provide an important technical result by showing how transverse TN contractions can be used to give access to Loschmidt echo in strongly correlated one-dimensional systems directly in the thermodynamic limit with a cost that only increases polynomially with the duration of the quench. Such echo can be used as a probe of quantum chaos and its behavior can be related to that of out-of-time ordered correlations [37] (for a review see e.g. [38]). The possibility to evaluate these quantities for arbitrarily long times is thus of paramount importance.

Setup and CFT predictions.— Given a 1D quantum system made by L constituents and described by a Hamiltonian H , we focus on the contraction of a tensor network encoding the Loschmidt echo, namely the return probability of a state of a quantum many-body system

* stefano.carignano@bsc.es

† luca.tagliacozzo@iff.csic.es

¹ For similar algorithms see also [31–35].

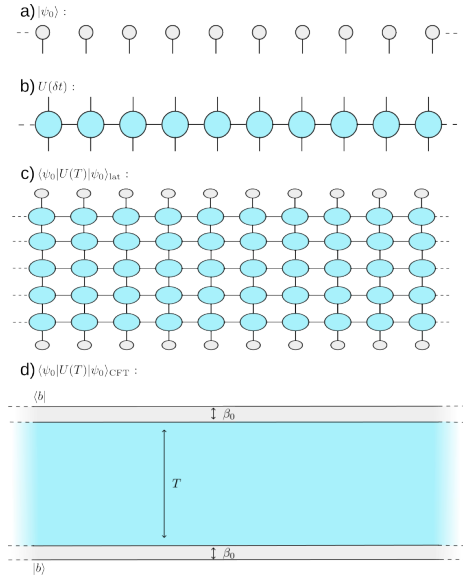


FIG. 1. The Loschmidt echo can be studied by analytically continuing the results obtained by mapping the CFT on the plane to appropriate finite geometry that depend on the initial state. The finite geometries are i) cylinders with diameter βv for an infinite temperature initial state or ii) strips with width βv . The infrared divergence are cured in the CFT by studying a finite spatial extent L that is then sent to $L \rightarrow \infty$

to its initial state after the out-of-equilibrium evolution for a time T , and its intensive part,

$$\mathcal{L} = |\langle \psi_0 | e^{-iHT} | \psi_0 \rangle|, \quad l = -\frac{\log \mathcal{L}}{TL}. \quad (1)$$

Such an intensive part is finite since the return probability decays exponentially to zero with both the size of the system and the temporal extent of the evolution. The quantity l thus plays the role of the free-energy in statistical mechanics.

Through simple tensor decompositions, we can express the evolution for an infinitesimal time step $U(\delta t)$ as a matrix product operator (MPO) with finite bond dimension (see e.g. [39, 40]), as shown in Fig. 1 b). As a result the full (1) is encoded by concatenating many of such steps and is given by the contraction of a regular 2D tensor network, made by $L \times N_T$ tensor ($N_T = T/\delta t$) elementary four-leg tensors, one for every space-time point (x, t) , as shown in Fig. 1 c). Since everything is translationally invariant, we can directly consider the thermodynamic limit by sending $L \rightarrow \infty$, thus building an infinite strip with a width of N_T tensors in the time direction, as represented in panel c) of Fig. 1.

We focus on critical dynamics and, in order to make contact with boundary conformal field theories (bcFT), we choose initial states obtained by evolving an initial product state in euclidean time β_0 [7–9]. The results of our calculation for initial product states are thus obtained by taking the limit $\beta_0 \rightarrow 0$, though in CFT such

limit could be singular. In CFT the initial states are conformally invariant boundary states $|b\rangle$ [9, 21] and the Loschmidt echo is described by a CFT in the geometry illustrated in Fig. 1 representing an infinite long strip with transverse size $T + 2\beta_0$ and with boundary conditions given by the chosen boundary states $|b\rangle$. The standard form of the evolution operator $\text{tr}(U(T))$ can also be considered by starting with the initial infinite temperature state, thus working with a CFT defined on infinitely long cylinders with circumference given by $T + 2\beta_0$.

Following well-known prescriptions [7, 8, 41], we obtain predictions for the real time calculations by performing an analytic continuation of the imaginary time results. We start with the standard results for CFTs on an infinite strip (for completeness, we recall analogous results for a cylinder in Appendix A) with imaginary extent β and analytically continue the results to the case $\beta = iT + 2\beta_0$ [7, 27, 28, 42].

As usual, the CFT predictions at finite β are obtained by using conformal maps². The infinite strip described by complex coordinate $w = s + iu$, related to the upper 2D plane by the conformal map $w' = \frac{v\beta}{\pi} \log(z)$, where v is the sound velocity.

The transfer operator \mathcal{T} produces translation along s . Such operator is given by $\mathcal{T} = \exp(\int du \mathbb{T}_{ss} \Delta s)$, where \mathbb{T} represents the stress-energy tensor of the CFT and Δs is the UV cutoff in the spatial direction. Since all these constructions are well known and described in the CFT literature here we will only cite the results relevant to our analysis. In particular, the relevant TMs for initial product states (open boundary conditions) are given by

$$\mathcal{T} = \exp \left[-\frac{\kappa_s}{\beta v} + \frac{\pi}{\beta v} L_0 \right], \quad (2)$$

where $\kappa_s = -\pi c \delta t / 24$, L_0 is the relevant generator of the Virasoro algebra and c is the central charge [43–48]. If we now define the $\{\lambda_i\}$ logarithms of the eigenvalues of \mathcal{T} , one can see that the intensive part l of the Loschmidt echo is thus related to λ_0 , the logarithm of the leading eigenvalue of \mathcal{T} , namely $l \rightarrow -\frac{|\lambda_0|}{T}$ in the thermodynamic limit for a gapped \mathcal{T} . Also as well known from the CFT literature, L_0 is diagonal in the basis of scaling field, and from CFT one can predict its full spectrum which is given by the operator content of the corresponding boundary CFT (bcFT) [20, 21].

Before proceeding to the analytical continuation of the above formulas, we need to consider the non-universal terms we would have on the lattice, coming from the normalization of the Hamiltonian and the boundary effects [22, 23]. In particular, on the lattice, the logarithm of the leading eigenvalue of \mathcal{T} scales as

$$\lambda_0^{CFT} = a\beta v + b + \frac{\kappa}{\beta v} + \mathcal{O}\left(\frac{1}{(\beta v)^2}\right), \quad (3)$$

² Explicit CFT predictions for the Loschmidt echo after local quenches have been obtained in [9].

where a plays the role of the non-universal ground state energy and b of the boundary contributions [22, 23].

In the following we will also need the results for the two point function,

$$\langle \phi(\omega_1) \phi(\omega_2) \rangle = \left(\frac{\pi}{p\beta v} \right)^{2x} \sin \left[\frac{\pi}{\beta v} (u_1 - u_2) \right]^{-2x}, \quad (4)$$

where u_1 and u_2 are the imaginary part of the two points considered, and $p = 1$ for the cylinder, $p = 2$ for the strip. In order to describe the scaling of the Tsallis entropies of order n associated with the reduced transition matrices, rather than primary operators we need the correlators of twist fields [49–53], hence in the above formula x is substituted by $\Delta_n = \frac{c}{24} (n - 1/n)$ ³.

The analytic continuation of Eq. (4) provides the prediction for the traces of the n -th power of the reduced transition matrices, defined as

$$\mathcal{T}_t^{L|R} = \text{tr}_{N_t-t} \left[\mathcal{T}^{L|R} \right], \quad \mathcal{T}^{L|R} = \frac{|R\rangle \langle L|}{\langle L|R\rangle}, \quad (5)$$

where $|R\rangle$ and $\langle L|$ are the right and left eigenvectors of \mathcal{T} with the largest modulus.

From the analytic continuation of Eq. (3), we find

$$\text{Re}(\lambda_0^{CFT}) = 2\beta_0 av + b + \mathcal{O}\left(\frac{1}{T^2}\right), \quad (6)$$

$$\text{Im}(\lambda_0^{CFT}) = avT - \frac{\kappa}{vT} + \mathcal{O}\left(\frac{1}{T^2}\right). \quad (7)$$

The critical exponents of the CFTs dictate also the gaps of \mathcal{T} . Such gaps are given by the standard operator content for the cylinder, and the operator content of the bcFT for the strip. The latter depends on the boundary conditions [21, 54] and will be discussed for the specific models later. For the first gap, we find

$$\begin{aligned} \text{Re}(\lambda_1 - \lambda_0) &= \mathcal{O}\left(\frac{1}{T^2}\right), \\ \text{Im}(\lambda_1 - \lambda_0) &= -\frac{p\pi x_1}{vT} + \mathcal{O}\left(\frac{1}{T^2}\right), \end{aligned} \quad (8)$$

where x_1 is the smallest boundary critical exponent and once again we put as $\mathcal{O}(1/T^2)$ unknown higher-order terms from the CFT expansion. The CFT predictions extend to the whole spectrum of \mathcal{T} , resulting in a series of gaps which shrink to zero as T increases, as dictated by the various critical exponents of the theory [21]. These results unveil a connection between the CFTs and dual unitary evolutions, up to higher order corrections, which vanish as T increases, \mathcal{T} has full sectors of gaps that are purely imaginary, and collapse on the unit circle for $\beta_0 \rightarrow 0$. This suggests that \mathcal{T} becomes unitary in the limit of $T \rightarrow \infty$.

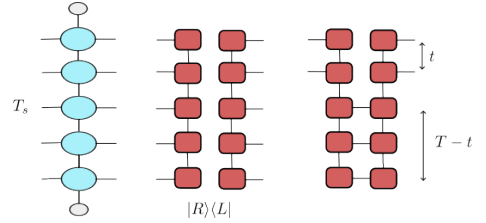


FIG. 2. By constructing a transverse transfer matrix \mathcal{T} as the construction of a column of elementary tensors a), and studying its leading left and right eigenvectors b) we can directly characterize the Loschmidt echo (1) in the thermodynamic limit. Generalized temporal entropies are extracted by the reduced transition matrices defined in (5).

Finally, by analytically continuing the results for the Tsallis entropies to $n = 1$ we can obtain the result for the generalized von Neumann entropies computed from the leading $|R\rangle$ and $\langle L|$ eigenvectors of \mathcal{T} . In the limit of small β_0 , from Eq. (4) we can replace $\beta \rightarrow iT$, $u_1 - u_2 \rightarrow it$ and we obtain

$$S_{gen} = s_0 + \frac{i\pi c}{12} + \frac{c}{6} \log \left[\frac{2T}{\pi} \sin \left(\frac{\pi t}{T} \right) \right], \quad (9)$$

with s_0 a constant. Interestingly, despite the fact that \mathcal{T} has purely imaginary gaps, as expected for a unitary operator, the leading eigenvectors only have generalized entropies which increase logarithmically with T . This fact is due to the CFT Hilbert space structure, whose number of states (at low energy) only diverges polynomially with T . In order to obtain such a simplification it is possibly important to consider a finite β_0 and only take $\beta_0 \rightarrow 0$ after taking the thermodynamic limit, for similar observations see also [41, 55, 56].

Similar predictions for the generalized entropies had been already obtained with different techniques based on holography and CFT in [26, 28, 42, 57] and thus our numerical results also help confirming such predictions.

We now check the above results using matrix product states (MPS). As in standard tensor network approaches, we define a transfer-matrix temporal MPO (tMPO) \mathcal{T} by contracting a vertical strip of tensors, and find its leading left and right eigenvectors in the form of temporal MPS (tMPS) [31–35, 58] as shown in Fig. 2. Our \mathcal{T} is thus defined by contracting one column of the infinite tensor network, containing $N_T + 2N_\beta$ (with $N_\beta = \beta_0/\delta t$) tensors.

For a gapped \mathcal{T} , as said the intensive Loschmidt echo converges exponentially fast to $l = -|\lambda_0|/T$ and in order to extract λ_0 we use an MPS ansatz for its eigenvectors of \mathcal{T} . The MPS approximation of $|R\rangle$ and $\langle L|$ are obtained in the gauge in which $\bar{\mathcal{T}} = \mathcal{T}^t$ (where the bar denotes complex conjugation), which is possible for the models considered here (see App. B). We can thus focus on extracting $|R\rangle$ and then obtain $\langle L| = \langle \bar{R}|$ by a simple transposition.

The concrete algorithm was introduced in [36] inspired on those presented in [31, 33]. It is basically a power method that iteratively applies the transfer matrix \mathcal{T} to

³ Notice that the sine in Eq. (4) is the result of the choice of the cut in the path integral, giving rise to the temporal reduced transition matrices that thus lie in the time direction.

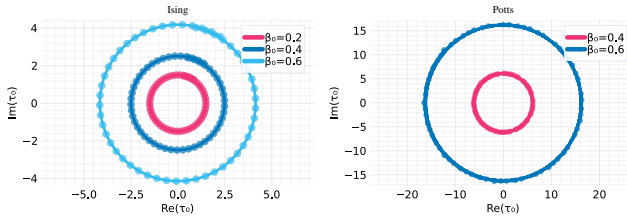


FIG. 3. Real vs imaginary parts of the dominant eigenvalue τ_0 of \mathcal{T} for various values of T and β_0 for the Ising (left) and Potts (right) models. For a fixed β_0 , as we vary T they lie on an almost constant radius circle as predicted from Eq. (7).

an initial MPS state and uses a low rank approximation of the reduced transition matrices in order to compress the MPS.

Numerical results.— For our numerical checks we consider both the transverse field Ising model with Hamiltonian

$$H_{\text{Ising}}(g) = - \sum_i \left[\sigma_x^i \sigma_x^{i+1} + g \sigma_z^i \right], \quad (10)$$

where σ_x, σ_z are the Pauli matrices, as well as the three-state Potts model defined via

$$H_{\text{Potts}}(g) = - \sum_i \left[\left(\sigma_i \sigma_{i+1}^\dagger + \sigma_i^\dagger \sigma_{i+1} \right) + g (\tau_i + \tau_i^\dagger) \right], \quad (11)$$

with the matrices $\sigma = \sum_{s=0,1,2} \omega^s |s\rangle \langle s|$, $\omega = e^{i2\pi/3}$ and $\tau = \sum_{s=0,1,2} |s\rangle \langle s+1|$, where the addition is considered modulo 3. In both cases, we work at the critical point ($g = 1$) and consider different lengths of the tMPO depending on T , which acts as IR cutoff, investigating also the dependence of our results on β_0 that works as a UV cutoff. We will consider $\delta t = 0.1$ as Trotter steps throughout.

Transfer matrix spectra. As we vary the length of the tMPO \mathcal{T} , its dominant eigenvalues $\tau_0(T)$ become distributed over circles (see Fig. 3), whose radius quickly collapses to a constant (depending on the value of β_0 as we vary T , consistent with the CFT predictions of Eq. (7). The same equation suggests to extract the central charge from the imaginary parts of its logarithm. More specifically, we fit $\text{Im}(\lambda_0)/T$ with a form $f_1(T) = a_0 + \kappa/T^2 + a_4/T^4$, focusing on the value of κ to extract c (cfr. Eq. (7)).

Our fits for different values of the regulator β_0 are shown in Fig. 4. All of them give comparable results for the relevant coefficients, more specifically for Ising we obtain $a_0 \approx 1.27$ and $\kappa \approx 0.032$, which when comparing to Eq. (7) using $v = 2$ for the sound velocity [58], gives $c_{\text{fit}} = 0.49$, in excellent agreement with the CFT prediction $c_{\text{Ising}} = 1/2$. For Potts, the fits give $\kappa \approx 0.039$, so that if we take into account a velocity $v_P \approx 3\sqrt{3}/2$ [59] we obtain a value $c_{\text{fit}} \approx 0.78$, compatible with the expected central charge $c_{\text{Potts}} = 4/5$. A similar analysis for the real part of the dominant eigenvalue also confirms the CFT predictions and is reported in App. C.

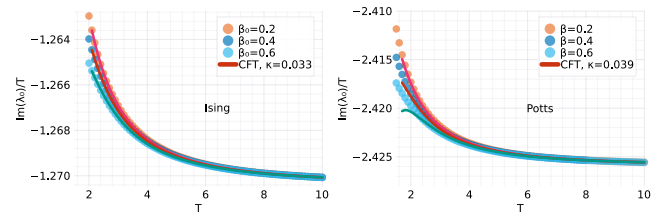


FIG. 4. Imaginary parts of λ_0 for different values of β_0 for the Ising (left) and Potts (right) models. The points are data from our TN calculation, solid lines are fits using the expected form from CFT (cfr. Eq. (7)), which we use to extract the value of the central charge (see main text). The fits show an excellent agreement with data for larger T , as expected.

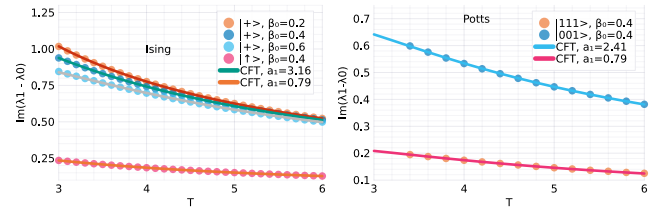


FIG. 5. Imaginary part of the gaps $\lambda_1 - \lambda_0$. Left: Results for the Ising model, obtained using different initial states, that correspond to free and fixed bCFT, and values of β_0 , as function of T . The points are the results of our TN calculation, the solid lines are fits using CFT formulas which are used to extract the exponent x_1 (see main text). Right: gaps for the Potts model using two different initial states, showing again the excellent agreement with the CFT expectations of the corresponding free and fixed bCFT.

Next, we compute the first excitation λ_1 of \mathcal{T} and extract the first gap. Focusing again on the imaginary parts, we fit $\text{Im}(\lambda_1 - \lambda_0)$ with a form $f_3(T) = a_1/T + a_3/T^3$, inspired by Eq. (8). Results are shown in Fig. 5: for the Ising model, we obtain $a_1 \approx 3.155$, which is in excellent agreement with the expected value $\pi x_1/v$ for $v = 2, x_1 = 2$. As a further check, we perform the same fits with a different initial state, namely $|\uparrow\rangle$ instead of $|\rightarrow\rangle$. For the fit coefficients we now get $a_1 = 0.786 \approx \pi/4$, which is consistent with $x_1 = 1/2$. The quoted values are the Ising bCFT predictions for the gap with fixed and free boundary conditions [21].

For Potts, we obtain $a_1 \approx 0.788$ for a $|111\rangle/\sqrt{3}$ initial state and $a_1 \approx 2.41$ for $|001\rangle$ state, corresponding to free and fixed boundary conditions, respectively. This corresponds to $x_1 = v_P a_1/\pi \approx 0.65$ and 1.98 , which we can match with the expected $2/3$ for the free and 2 for fixed boundary conditions [21, 54].

Generalized entropies. Our next step is to compute the generalized entropies obtained from the dominant eigenvectors of the transfer matrix, considering separately their real and imaginary parts. Such entropies are important since they have an holographic meaning [24–30, 60], and they are a measure for the complexity of the TN contraction and thus tell us the cost for simulating

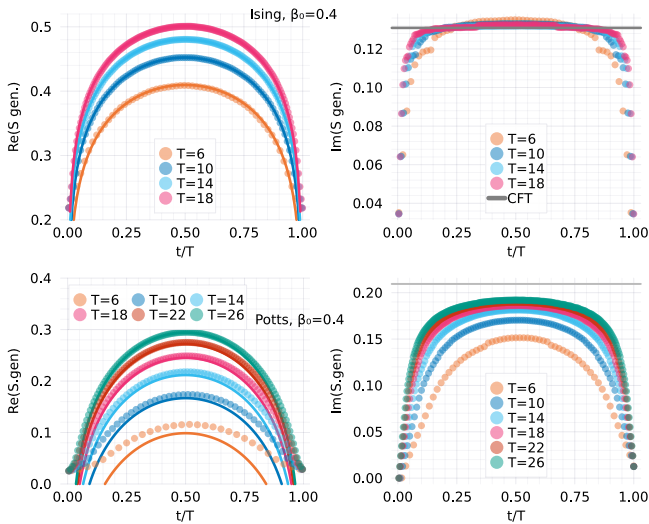


FIG. 6. Top: Numerical results for the real (left) and imaginary (right) parts of the generalized entropies for the critical Ising model. Thick solid lines denote the CFT predictions (9), with $c = 1/2$ the Ising central charge and $s_0 = 0.3$ the constant providing the best fit for the real part. The agreement with the CFT predictions is excellent for both real and imaginary parts, and it improves as we go to longer chains, as expected. Bottom: Numerical results for the real (left) and imaginary (right) parts of the generalized entropies for the critical three-state Potts model. Thick solid lines denote the CFT predictions (9), with $c_P = 4/5$ the central charge and $s_0 = -0.08$ the constant providing the best fit for the real part. The agreement with the CFT predictions improves for longer chains, but the imaginary part does not reach the expected result even for the longest chains considered, suggesting that the convergence is very slow, as discussed in App. D

the Loschmidt echo with tensor networks [31, 33, 35, 36]. We plot our results in Fig. 6. There we can see that for Ising the agreement with CFT predictions is excellent already for relatively short lengths of the TM: in particular, we note how - aside from boundary effects - the imaginary part becomes constant and matches the prediction $Im(S_{\text{CFT}}) = \pi c_{\text{Ising}}/12$, while the real part is well fitted by Eq. (9). The curves for Potts on the other hand start converging to the CFT predictions only for larger values of T , and the results for the imaginary parts still exhibit significant deviations even for the largest chains considered. In the Appendix D we show how this is consistent with the presence of extra finite-size scaling corrections.

Conclusions. — We have shown that the time evolution operator generated by a critical Hamiltonian gives rise to a unitary transfer matrix in space, something that one would expect for dual unitary evolutions. Conformal symmetry thus seems to imply emerging dual unitarity. This is just one of the results we obtain by extracting the CFT predictions for the Loschmidt echo after a global quench. All of those predictions are confirmed by state-of-the-art numerical simulations. In particular we have focused on the role of both UV and IR regulators on the

scaling of the generalised temporal entropies, since we observe a special class of transverse unitary evolution, whose leading eigenvectors have only logarithmically increasing entropies, possibly due to our ultra-violet regularization of the dynamics by means of an infinitesimal euclidean evolution β_0 . In other contexts [41, 55, 56] similar observations were made and our work provides some analytical insight that could be extended to such scenarios. From a more technical side, our results also open the way to applying tensor networks in those contexts and provide definite answers to open problems along the lines of the recent approaches [61–66].

Acknowledgements. — We would like to thank M.C. Bañuls, P. Calabrese, E. Lopez, G. Sierra, E. Tonni for discussions related to this project. LT acknowledge support from the Proyecto Sinérgico CAM Y2020/TCS-6545 NanoQuCo-CM, the CSIC Research Platform on Quantum Technologies PTI-001, and from the Grant TED2021-130552B-C22 funded by MCIN/AEI/10.13039/501100011033 and by the “European Union NextGenerationEU/PRTR”, and Grant PID2021-127968NB-I00 funded by MCIN/AEI/10.13039/501100011033.

Appendix A: CFT predictions for a cylinder

For completeness, we recall here CFT predictions for an infinite temperature boundary state, which would result in an infinite cylinder geometry. From the TN point of view, we can represent it using the same algorithm employed in this manuscript by folding the cylinder, similar to what proposed in [31]. The infinite cylinder described by complex coordinate $w = s + iu$, related to the 2D plane by the conformal map $w = \frac{v\beta}{2\pi} \log(z)$, and the transfer operator in this case is given by

$$\mathcal{T} = \exp \left[-\frac{\kappa}{\beta v} + \frac{2\pi}{\beta v} (L_0 + \bar{L}_0) \right], \quad (\text{A1})$$

where $\kappa = -\pi c \delta t / 6$. We will present the corresponding numerical results elsewhere.

Appendix B: TN setup, symmetric MPO

In this section we briefly describe the methods used in this work for building the MPO of the transition matrix \mathcal{T} and extract its eigenvalues. The basic ingredients for the MPO are the tensors $W_i(\delta t)$ associated with a given site and timestep, building up the time evolution operator $U(\delta t)$ (see Fig. 1). Since we work with translationally invariant systems, there is no explicit space dependence, and all tensors have the same dependence on δt . The only inhomogeneities in the time direction are induced by the initial state $|\psi_0\rangle$, which we take as a product state.

In principle, the roles of virtual and physical legs are interchanged if one performs a transverse contraction, as

the temporal MPO \mathcal{T} is applied sideways to the boundary MPS which will result in the dominant left and right vectors. In this sense, an asymmetry in the virtual legs of the MPO tensors will result in a left dominant vector for \mathcal{T} which is different from the right one, ie. $|L\rangle \neq |R\rangle$. Nevertheless, as mentioned in the main text, for the models considered here we were able to work with tensors which are symmetric on both the physical and virtual legs, so that this additional complication does not arise. Being able to work with symmetric left-right \mathcal{T} also significantly improves the numerical stability of our TN simulations (see eg. [67] and references therein for a discussion on the challenges presented by non-hermitian eigenvalue problems).

More specifically, for the Ising model we employ the compact representation proposed in [40], for which we obtain, at second-order in the Trotter expansion,

$$W_{Ising} = \begin{pmatrix} \cos(\delta t)(a\mathbf{1} + b\sigma_z) & \sqrt{i \sin(\delta t) \cos(\delta t)} \sigma_x \\ \sqrt{i \sin(\delta t) \cos(\delta t)} \sigma_x & i \sin(\delta t)(a\mathbf{1} + b\sigma_z) \end{pmatrix}, \quad (\text{B1})$$

with $a = 1 - 2 \sin(g\delta t/2)^2$, $b = 2i \sin(g\delta t/2) \cos(g\delta t/2)$.

The generalization of this type of construction unfortunately would not lead to a symmetric left-right MPO in the case of the Potts model, due to the presence of both σ_i and σ_i^\dagger terms (cfr. Eq. (11)). Nevertheless, we are still able to extract a symmetric expression by considering the two-body operator $U_{i,i+1}(\delta t)$ and separating it via a symmetric SVD factorization. The resulting MPO tensors are again symmetric in both physical and virtual legs.

Having obtained the form of the transfer matrix tensors, we build the transverse MPO for \mathcal{T} by building N_β steps of imaginary time ($\delta t \rightarrow -i\delta\beta_0$) at the edges of the TM, whereas the real time evolution is performed in the center.

The determination of the dominant eigenvalues of \mathcal{T} was performed via a symmetric power method algorithm which simply goes as follows: starting from an initial guess for the right dominant vector $|R\rangle$ in the form of MPS along the temporal direction, at each iteration \mathcal{T} is applied to $|R\rangle$ and the resulting MPS is truncated by optimizing the overlap $\langle \bar{R} | R \rangle$, since, as already discussed, in our case we have $\langle L | = \langle \bar{R} |$. This is done by appropriately truncating on the singular values of the reduced transition matrices, Eq. (5) (see [36] for additional details). The iterations are repeated until convergence is reached, and the eigenvalues of the transition matrices are used to compute the entropies along the temporal chains.

Appendix C: Fits on real parts of the dominant eigenvalues.

By fitting the real part of the dominant eigenvalues of \mathcal{T} we can get further confirmation of our CFT predictions, although the procedure is a bit more involved. When it comes to the real parts, by comparing with Eq. 7, we see that a single term $a_0 = 2\beta_0 av + b$ does not allow us to resolve the pieces involved, but we can extract some additional information by looking at the difference of the real parts for different values of β_0 . Indeed, if we consider $\Delta_\beta \lambda_0 \equiv \lambda_0^{\beta_0 \equiv \beta_1} - \lambda_0^{\beta_0 \equiv \beta_2}$, we expect that $Re(\Delta_\beta \lambda_0) = 2a(\beta_1 - \beta_2) + \mathcal{O}(1/T^2)$, whereas $Im(\Delta_\beta \lambda_0) = \mathcal{O}(1/T^3)$.

We thus fit the difference of the real part for different values of β with a functional form $f_2 = b_0 + b_2/T^2$. As an example, we fit for the Ising model, for the case $\Delta_\beta \lambda_0(\beta = 0.4 - \beta = 0.2)$ we get $b_0 = 0.51$, whereas for $\Delta(\beta = 0.6 - \beta = 0.2)$ we find $b_0 = 1.02$, showing again an excellent agreement with the CFT prediction which indeed gives a ratio of 2 between the two values.

At this point, we can also extract the non-universal coefficient $a = b_0/2(\beta_1 - \beta_2) \approx 1.275$ from here, which is consistent with the a_0 from the fit of the imaginary part above.

Appendix D: Corrections to the leading finite size scaling

Upon inspecting Fig. 6, it seems that for the case of the Potts model there are still significant deviations between the CFT predictions of the imaginary part of the generalized temporal entropy and what we actually extract from the lattice simulations⁴. Such large deviations are quite usual in the context of studying the scaling of the entanglement entropy in different scenarios [68–72]. Here we show that even in this case such corrections are induced by standard finite size effects and vanish as inverse powers of the IR cutoff. In our case, we expect both a finite β_0 and T to introduce perturbations to our system. For T we can use the standard analysis described in the paper [68]. The CFT corrections should scale as some inverse power of $\delta S \propto T^{-x}$, with x the lowest neutral relevant field. This implies that for Ising $x = 1 = \Delta_\epsilon$ while for Potts this should be $x = 4/5 = \Delta_\epsilon$. Our numerical results confirm such type of corrections.

Now we can add the effects of finite β_0 . Since β_0 plays the role of a UV cut-off, we now expect corrections $\delta S \propto \beta_0^\gamma$ with γ the scaling dimension of the most relevant operator coupling to δS . We find that for Ising $\gamma = 1.5$ which is compatible with $\gamma = 2 - \Delta'_\sigma$, where here $\Delta'_\sigma = 0.5$ the boundary magnetization.

For Potts on the other hand we find $\gamma \simeq 0.3$ and we do not have a clear understanding on where it could come from even though it could be $\gamma = 2 - (1 + \delta_{1,2}) = 2 - (1 + 2/3)$.

Putting everything together we thus expect that the scaling variable for the correction should be $\frac{\beta_0^{\gamma/x}}{T}$. Our analyses are presented in Fig. 7

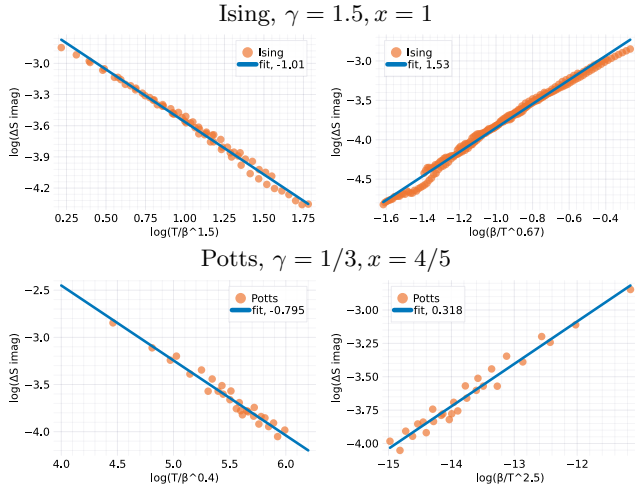


FIG. 7. Scaling behavior for ΔS , the difference of the imaginary part (at mid-chain) of the Ising (first row) and Potts (middle, bottom rows) entropies with the respect to the CFT predictions. ΔS for the various cases are plotted as function of $T/\beta_0^{\gamma/x}$ (left) and of $\beta_0/T^{x/\gamma}$ (right). The situation for finite T effects is clear and coincide with the prediction of [68] in which for both Potts and Ising $x = \Delta_\epsilon$. Finite β_0 effects are unusual. For Ising we find β_0 being responsible of the appearance of the boundary magnetization. For Potts, the situation is less clear: $\gamma \simeq 1/3$ works but does not have a clear interpretation with $1/3$ being compatible with $2 - (1 + \Delta_{1,2})$

-
- [1] JCCMP, Whither many-body localization? (2023).
- [2] A. Chandran and P. Crowley, *Physics* **17**, 24 (2024).
- [3] J.-S. Caux and F. H. L. Essler, *Phys. Rev. Lett.* **110**, 257203 (2013).
- [4] F. H. L. Essler and A. J. J. M. de Klerk, *Statistics of matrix elements of local operators in integrable models* (2023), [arxiv:2307.12410](https://arxiv.org/abs/2307.12410) [cond-mat].
- [5] B. Bertini, M. Collura, J. De Nardis, and M. Fagotti, *Phys. Rev. Lett.* **117**, 207201 (2016).
- [6] O. A. Castro-Alvaredo, B. Doyon, and T. Yoshimura, *Phys. Rev. X* **6**, 041065 (2016).
- [7] P. Calabrese and J. Cardy, *J. Stat. Mech.* **2005**, P04010 (2005).
- [8] P. Calabrese and J. Cardy, *J. Stat. Mech.* **2007**, P10004 (2007).
- [9] J.-M. Stéphan and J. Dubail, *J. Stat. Mech.* **2011**, P08019 (2011).
- [10] J. Cardy and E. Tonni, *J. Stat. Mech.: Theory Exp.* **2016** (12), 123103.
- [11] J. Dubail, *J. Phys. A: Math. Theor.* **50**, 234001 (2017), [arxiv:1612.08630](https://arxiv.org/abs/1612.08630) [cond-mat, physics:hep-th, physics:quant-ph].
- [12] J. Surace, L. Tagliacozzo, and E. Tonni, *Phys. Rev. B* **101**, 241107 (2020).
- [13] A. Nahum, J. Ruhman, S. Vijay, and J. Haah, *Phys. Rev. X* **7**, 031016 (2017), [arxiv:1608.06950](https://arxiv.org/abs/1608.06950) [cond-mat, physics:hep-th, physics:quant-ph].
- [14] B. Bertini, P. Kos, and T. Prosen, *Phys. Rev. Lett.* **121**, 264101 (2018), [arxiv:1805.00931](https://arxiv.org/abs/1805.00931) [cond-mat, physics:hep-th, physics:nlin, physics:quant-ph].
- [15] B. Bertini, P. Kos, and T. Prosen, *Phys. Rev. X* **9**, 021033 (2019).
- [16] B. Bertini, P. Kos, and T. Prosen, *Phys. Rev. Lett.* **123**, 210601 (2019).
- [17] P. W. Claeys and A. Lamacraft, *Phys. Rev. Research* **2**, 033032 (2020), [arxiv:2003.01133](https://arxiv.org/abs/2003.01133) [cond-mat, physics:nlin, physics:quant-ph].
- [18] P. W. Claeys and A. Lamacraft, *Phys. Rev. Lett.* **126**, 100603 (2021), [arxiv:2009.03791](https://arxiv.org/abs/2009.03791) [cond-mat, physics:quant-ph].
- [19] L. Masanes, *Discrete holography in dual-unitary circuits* (2023), [arxiv:2301.02825](https://arxiv.org/abs/2301.02825) [cond-mat, physics:gr-qc, physics:hep-th, physics:quant-ph].
- [20] J. Cardy, *Nucl. Phys. B* **270**, 186 (1986).
- [21] J. L. Cardy, *Nuclear Physics B* **275**, 200 (1986).
- [22] J. L. Cardy, *J. Phys. A: Math. Gen.* **17**, L385 (1984).
- [23] I. Affleck, *Phys. Rev. Lett.* **56**, 746 (1986).
- [24] K. Narayan, *Phys. Rev. D* **91**, 126011 (2015), [arxiv:1501.03019](https://arxiv.org/abs/1501.03019) [gr-qc, physics:hep-th].
- [25] K. Narayan, *Physics Letters B* **753**, 308 (2016), [arxiv:1504.07430](https://arxiv.org/abs/1504.07430) [hep-th].
- [26] Y. Nakata, T. Takayanagi, Y. Taki, K. Tamaoka,

⁴ A slow convergence of the Potts model results to the continuum limit was already observed in Ref. [41].

- and Z. Wei, *Phys. Rev. D* **103**, 026005 (2021), [arxiv:2005.13801](#) [cond-mat, physics:hep-th, physics:quant-ph].
- [27] K. Doi, J. Harper, A. Mollabashi, T. Takayanagi, and Y. Taki, *Timelike entanglement entropy* (2023), [arxiv:2302.11695](#) [cond-mat, physics:hep-th, physics:quant-ph].
- [28] K. Doi, J. Harper, A. Mollabashi, T. Takayanagi, and Y. Taki, *Phys. Rev. Lett.* **130**, 031601 (2023), [arxiv:2210.09457](#) [cond-mat, physics:hep-th, physics:quant-ph].
- [29] K. Narayan and H. K. Saini, *Notes on time entanglement and pseudo-entropy* (2023), [arxiv:2303.01307](#) [hep-th].
- [30] Z. Li, Z.-Q. Xiao, and R.-Q. Yang, *J. High Energ. Phys.* **2023** (4), 4, [arxiv:2211.14883](#) [gr-qc, physics:hep-th].
- [31] M. C. Bañuls, M. B. Hastings, F. Verstraete, and J. I. Cirac, *Phys. Rev. Lett.* **102**, 240603 (2009).
- [32] A. Müller-Hermes, J. I. Cirac, and M. C. Bañuls, *New J. Phys.* **14**, 075003 (2012), [arxiv:1204.5080](#) [cond-mat, physics:quant-ph].
- [33] M. B. Hastings and R. Mahajan, *Phys. Rev. A* **91**, 032306 (2015), [arxiv:1411.7950](#) [cond-mat, physics:hep-th, physics:quant-ph].
- [34] A. Lerose, M. Sonner, and D. A. Abanin, *Phys. Rev. X* **11**, 021040 (2021).
- [35] A. Lerose, M. Sonner, and D. A. Abanin, *Phys. Rev. B* **107**, L060305 (2023).
- [36] S. Carignano, C. R. Marimón, and L. Tagliacozzo, *On temporal entropy and the complexity of computing the expectation value of local operators after a quench* (2023), [arxiv:2307.11649](#) [cond-mat, physics:quant-ph].
- [37] B. Yan, L. Cincio, and W. H. Zurek, *Phys. Rev. Lett.* **124**, 160603 (2020), [arxiv:1903.02651](#) [quant-ph].
- [38] A. Goussev, R. A. Jalabert, H. M. Pastawski, and D. Wisniacki, *Scholarpedia* **7**, 11687 (2012), [arxiv:1206.6348](#) [cond-mat, physics:quant-ph].
- [39] I. P. McCulloch, *J. Stat. Mech.* **2007**, P10014 (2007).
- [40] B. Pirvu, V. Murg, J. I. Cirac, and F. Verstraete, *New J. Phys.* **12**, 025012 (2010).
- [41] N. F. Robertson, J. Surace, and L. Tagliacozzo, *Phys. Rev. B* **105**, 195103 (2022), [arxiv:2110.07078](#) [cond-mat, physics:hep-th, physics:quant-ph].
- [42] W.-z. Guo, S. He, and Y.-X. Zhang, *Relation between timelike and spacelike entanglement entropy* (2024), [arxiv:2402.00268](#) [cond-mat, physics:hep-th, physics:quant-ph].
- [43] A. A. Belavin, A. M. Polyakov, and A. B. Zamolodchikov, *Nuclear Physics B* **241**, 333 (1984).
- [44] J. Cardy, *Lectures Cardy Les Houches 88* (1988).
- [45] P. Ginsparg, [arXiv:hep-th/9108028](#) (1988), [arxiv:hep-th/9108028](#).
- [46] P. Francesco, P. Mathieu, and D. Sénéchal, *Conformal Field Theory*, Graduate Texts in Contemporary Physics (Springer-Verlag, New York, 1997).
- [47] M. Henkel, *Conformal Invariance and Critical Phenomena*, Theoretical and Mathematical Physics (Springer-Verlag, Berlin Heidelberg, 1999).
- [48] J. Cardy, [0807.3472](#) (2008), [arxiv:0807.3472](#).
- [49] M. Srednicki, *Phys. Rev. Lett.* **71**, 666 (1993).
- [50] C. Callan and F. Wilczek, [arXiv:hep-th/9401072](#) [10.1016/0370-2693\(94\)91007-3](#) (1994), [arxiv:hep-th/9401072](#).
- [51] G. Vidal, J. I. Latorre, E. Rico, and A. Kitaev, *Phys. Rev. Lett.* **90**, 227902 (2003).
- [52] P. Calabrese and J. Cardy, *J. Stat. Mech.* **2004**, P06002 (2004).
- [53] M. Caraglio and F. Gliozzi, *J. High Energy Phys.* **2008** (11), 076, [arxiv:0808.4094](#) [cond-mat, physics:hep-lat, physics:hep-th].
- [54] I. Affleck, M. Oshikawa, and H. Saleur, *J. Phys. A: Math. Gen.* **31**, 5827 (1998).
- [55] M. Grundner, P. Westhoff, F. B. Kugler, O. Parcollet, and U. Schollwöck, *Complex Time Evolution in Tensor Networks* (2023), [arxiv:2312.11705](#) [cond-mat, physics:quant-ph].
- [56] X. Cao, Y. Lu, E. M. Stoudenmire, and O. Parcollet, *Dynamical correlation functions from complex time evolution* (2024), [arxiv:2311.10909](#) [cond-mat].
- [57] W.-z. Guo, S. He, and Y.-X. Zhang, *J. High Energ. Phys.* **2022** (9), 94, [arxiv:2206.11818](#) [hep-th].
- [58] E. Tirrito, N. J. Robinson, M. Lewenstein, S.-J. Ran, and L. Tagliacozzo, *Characterizing the quantum field theory vacuum using temporal Matrix Product states* (2022), [arxiv:1810.08050](#) [cond-mat].
- [59] A. A. Eberharter, L. Vanderstraeten, F. Verstraete, and A. M. Läuchli, *Phys. Rev. Lett.* **131**, 226502 (2023).
- [60] K. Shinmyo, T. Takayanagi, and K. Tasuki, *Pseudo entropy under joining local quenches* (2023), [arxiv:2310.12542](#) [cond-mat, physics:hep-th, physics:quant-ph].
- [61] J. Surace, M. Piani, and L. Tagliacozzo, *Phys. Rev. B* **99**, 235115 (2019).
- [62] A. Strathearn, P. Kirton, D. Kilda, J. Keeling, and B. W. Lovett, *Nat Commun* **9**, 3322 (2018).
- [63] C. D. White, M. Zaletel, R. S. K. Mong, and G. Refael, *Phys. Rev. B* **97**, 035127 (2018), [arxiv:1707.01506](#) [cond-mat].
- [64] T. Rakovszky, C. W. von Keyserlingk, and F. Pollmann, *Dissipation-assisted operator evolution method for capturing hydrodynamic transport* (2020), [arxiv:2004.05177](#) [cond-mat].
- [65] M. Frías-Pérez and M. C. Bañuls, *Phys. Rev. B* **106**, 115117 (2022), [arxiv:2201.08402](#) [quant-ph].
- [66] W.-Y. Liu, S.-J. Du, R. Peng, J. Gray, and G. K.-L. Chan, *Tensor Network Computations That Capture Strict Variationality, Volume Law Behavior, and the Efficient Representation of Neural Network States* (2024), [arxiv:2405.03797](#) [cond-mat, physics:physics, physics:quant-ph].
- [67] W. Tang, F. Verstraete, and J. Haegeman, *Matrix Product State Fixed Points of Non-Hermitian Transfer Matrices* (2023), [arxiv:2311.18733](#) [cond-mat, physics:quant-ph].
- [68] J. Cardy and P. Calabrese, *Journal of Statistical Mechanics: Theory and Experiment* **2010**, P04023 (2010).
- [69] V. Alba, L. Tagliacozzo, and P. Calabrese, *Physical Review B* **81**, 60411 (2010).
- [70] V. Alba, L. Tagliacozzo, and P. Calabrese, *Journal of Statistical Mechanics: Theory and Experiment* **06**, 012 (2011).
- [71] P. Calabrese, L. Tagliacozzo, and E. Tonni, *J. Stat. Mech.* **2013**, P05002 (2013).
- [72] A. Coser, L. Tagliacozzo, and E. Tonni, *J. Stat. Mech.* **2014**, P01008 (2014).